Reaction Coordinate and Rate Constants for Nitrous Acid cis−trans Isomerization

Glauco F. Bauerfeldt, Graciela Arbilla,* and Edilson Clemente da Silva

Departamento de Físico-Química—Instituto de Química, Universidade Federal do Rio de Janeiro, Centro de Tecnologia, Bloco A, Cidade Universitária, 21949-900, Rio de Janeiro, RJ, Brazil

Received: May 9, 2000; In Final Form: July 20, 2000

Nitrous acid is one of the simplest molecules that undergoes geometric isomerization. The reaction path properties and rate constants of isomerization have been determined at the MP2 and DFT levels of theory. Good agreement is obtained with experimental data. The calculated isomerization threshold energy is 10.8−12.0 kcal/mol, and the experimental value is 11.6 ± 0.2 kcal/mol. The microcanonical RRKM rate constants, which include the effects of the variational transition state and the *J* rotational quantum number, are calculated. High-pressure rate constants are determined for the 223−323 K temperature range.

Introduction

Nitrous acid (HONO) is one of the simplest molecules that undergoes cis−trans isomerization. Both cis and trans conformers have been experimentally detected, and the molecular geometries were determined using microwave spectroscopy.[1] The isomerization has been extensively studied as a laser-induced conversion and by monitoring the torsion mode in the infrared spectrum.[2−4] The torsion barrier, *V*, may be determined by fitting the data with torsion angle cosine functions[5−7]

$$V(\alpha) = \sum_n V_n \cos(\alpha_n)$$

and the gauche angle, α_{max}, may be estimated as the angle that maximizes the energy. These potentials only take into account the energy difference between the stable isomers and the energy barrier for the reaction, so they are not able to describe the process as a whole, and they constitute a poor approximation to the minimum energy path for isomerization.

Post Hartree−Fock calculations using coupled cluster methods have been performed[8] to determine the molecular properties of the cis and trans isomers. The isomerization reaction was studied theoretically at the Hartree−Fock,[9−13] MP_n (n = 2−4),[14,15] and GVB[15] levels, but to the best of our knowledge, an accurate ab initio reaction coordinate is not available. The effect of the basis set on the rotational barrier was evaluated,[16] and the 6-31G basis with polarization functions at least was recommended.

The rate constants for nitrous acid isomerization were first estimated[17] using transition state theory. In that work,[17] the molecular properties (geometry and frequencies) of the cis and trans isomers used in the calculations were taken from spectroscopy studies, and the corresponding properties for the transition state were determined as follows: a torsion barrier previously deduced from the infrared spectra was used to determine the gauche angle, and the remaining structural parameters were taken to be essentially intermediate between those of the cis and trans isomers; the principal moments of inertia were calculated, and the vibrational frequencies were evaluated from estimated force constants.

In the present paper, the geometric isomerization of nitrous acid was studied by the direct dynamics[18] method; this involves optimizing the geometries of reactants and products, and searching for a saddle point, and constructing an intrinsic reaction coordinate.[19] The points along the reaction path were analyzed in terms of geometric parameters and the variation of the vibrational frequencies. Then the data from the theoretical calculations were used to evaluate rate constants.

Computational Procedures

The calculations were performed using the second-order Møller−Plesset perturbation theory (MP2)[20] and the density functional theory (DFT).[21] For the latter, the B3LYP[22] hybrid functional was used. The basis sets D95V,[23] 6-31G,[24] and 6-311G[25] with polarization functions were considered in order to reach the most accurate dynamic description. The Hartree−Fock results were used in this work as the starting point for higher-level calculations.

The rate constants were evaluated in both canonical and microcanonical approaches following the Rice−Ramsperger−Kassel−Marcus (RRKM) theory.[26]

Results

1. Geometry Optimizations and Frequencies. The cis and trans isomers of nitrous acid are planar and have C_s symmetry. The geometries for these molecules were optimized with an algorithm proposed by Schlegel et al.,[27] as implemented in GAUSSIAN.[28]

The comparison between the calculated results and the experimental data[1] was carried out by considering the relative deviation of distances and angles. Calculation at the RHF/D95V-(d,p) level underestimates bond distances and overestimates the angles. MP2 results are satisfactory, with low relative deviations for distances and angles. The relative deviations of DFT results are even smaller. No significant differences in geometry were observed when the full-MP2/D95V(d,p) method was used. Less than 1% deviation is observed for the B3LYP results with 6-31G(d,p) and 6-311G(d,p) basis sets, which suggests that the use of the double-ζ basis provides good results, very similar to those obtained with the triple-ζ basis at less computational time. Also, the B3LYP and MP2 results are comparable to reported CCSD(T) data.[8]

In regard to the calculated saddle point geometry, an increase in the N−O bond distance and HNO and ONO angles and a decrease in the N═O bond distance are observed with respect

* Corresponding author. E-mail: graciela@iq.ufrj.br.

10.1021/jp001732g CCC: $19.00
Published on Web 10/26/2000

TABLE 1: Calculated and Experimental Geometric Parameters for *cis*-HONO, *trans*-HONO, and the Saddle Point[a]

		experimental[1]	RHF D95V(d,p)	MP2 D95V(d,p)	full-MP2 D95V(d,p)	MP2 6-31G(d,p)	B3LYP D95V(d,p)	B3LYP 6-31G(d,p)	B3LYP 6-311G(d,p)
cis-HONO	O−H	0.982	0.956	0.982	0.982	0.982	0.984	0.983	0.979
	N−O	1.392	1.328	1.394	1.393	1.387	1.394	1.384	1.388
	N═O	1.185	1.166	1.216	1.215	1.210	1.199	1.192	1.181
	HON	104.0	107.8	104.6	104.5	104.3	105.6	105.4	105.8
	ONO	113.6	113.6	112.6	112.6	112.7	113.1	113.2	113.6
	α	0.0	0.0	0.0	0.0	0.0	0.0	0.0	0.0
saddle point	O−H	−	0.950	0.974	0.974	0.973	0.975	0.973	0.969
	N−O	−	1.390	1.516	1.513	1.504	1.491	1.491	1.501
	N═O	−	1.154	1.192	1.191	1.187	1.178	1.170	1.157
	HON	−	107.2	102.6	102.7	102.3	104.3	104.0	103.9
	ONO	−	111.7	110.8	110.9	110.8	111.3	111.2	111.6
	α	−	88.0	87.5	87.5	87.5	88.1	88.0	87.4
trans-HONO	O−H	0.958	0.947	0.973	0.973	0.972	0.974	0.972	0.968
	N−O	1.432	1.347	1.433	1.432	1.425	1.430	1.426	1.433
	N═O	1.170	1.158	1.202	0.972	1.197	1.186	1.179	1.166
	HON	102.1	105.4	101.5	101.5	101.7	102.3	102.3	102.3
	ONO	110.7	111.4	110.2	110.2	110.3	110.6	110.6	111.0
	α	180.0	180.0	180.0	180.0	180.0	180.0	180.0	180.0

[a] Bond distances (O−H, N−O, e N═O) in Å and angles (HON, ONO, and α-torsional angle) in deg.

TABLE 2: Calculated Harmonic Vibrational Frequencies (cm^{-1}) for *cis*-HONO, *trans*-HONO, and the Saddle Point

		experimental[29]	RHF D95V(d,p)	MP2 D95V(d,p)	full-MP2 D95V(d,p)	MP2 6-31G(d,p)	B3LYP D95V(d,p)	B3LYP 6-31G(d,p)	B3LYP 6-311G(d,p)
cis-HONO	υ_{O-H}	3425	4037	3676	3678	3646	3611	3580	3587
	$\upsilon_{N=O}$	1640	1970	1601	1604	1619	1703	1725	1719
	υ_{N-O}	1261	1516	1330	1333	1345	1329	1349	1337
	δ_{HON}	853	1178	937	938	947	921	923	894
	δ_{ONO}	608	726	638	639	653	635	649	716
	τ_H	638	778	724	728	742	717	734	639
saddle point	υ_{O-H}	−	4125	3815	3819	3801	3768	3745	3756
	$\upsilon_{N=O}$	−	2018	1636	1641	1652	1770	1798	1805
	υ_{N-O}	−	1281	1067	1070	1091	1065	1079	1059
	δ_{HON}	−	1067	769	771	778	814	811	801
	δ_{ONO}	−	781	508	511	532	580	579	557
	τ_H	−	615*i*	600*i*	601*i*	611*i*	677*i*	684*i*	669*i*
trans-HONO	υ_{O-H}	3588	4171	3830	3833	3811	3778	3756	3775
	$\upsilon_{N=O}$	1699	2027	1640	1644	1657	1769	1792	1794
	υ_{N-O}	1265	1493	1287	1290	1302	1295	1306	1297
	δ_{HON}	791	1111	843	844	863	859	864	835
	δ_{ONO}	593	739	619	620	628	629	632	620
	τ_H	540	584	592	595	600	589	595	589

to the potential minima. The O−H bond distance does not significantly change, while the torsion angle is the internal coordinate that undergoes the largest variation and reaches approximately 88° at the saddle point. The geometric parameters of *cis*- and *trans*-HONO and saddle point are presented in Table 1.

Nitrous acid has six vibrational modes: stretching $\upsilon_{O-H}(A')$, stretching $\upsilon_{N=O}(A')$, bending $\delta_{HON}(A')$, stretching $\upsilon_{N=O}(A')$, bending $\delta_{ONO}(A')$, and torsion $\tau_H(A'')$. The harmonic vibrational frequencies were calculated and are presented in Table 2. The relative deviation criterion was used to compare the experimental frequencies[29] and theoretical data. Corrections for anharmonicity were not considered. The results with larger deviation are those obtained by the RHF method, with an average of 22% above the experimental value. The MP2 and B3LYP results show smaller relative deviations (5 and 6%, respectively). Again, no significant variation is observed with the change of the basis set. At the saddle point, one of the vibrational modes is lost due to a negative eigenvalue in the Hessian matrix. As a result, an imaginary frequency is obtained for this structure, as presented in Table 2. A simple normal coordinate analysis shows that this imaginary frequency is related to the torsion mode.

The calculated energies for *cis*-HONO, *trans*-HONO, and the saddle point are presented in Table 3. The enthalpy, entropy, and free energy of reaction (ΔH, ΔS, and ΔG) were calculated at 298.15 K on the basis of the difference between *cis*-HONO and *trans*-HONO. The activation parameters (critical energy E_0, activation entropy $\Delta S^{\ddagger}$, and Gibbs energy $\Delta G^{\ddagger}$) were calculated on the basis of the thermodynamic properties of the saddle point and *trans*-HONO.

The energy differences between the isomers show that the cis conformer is slightly more stable. Calculated critical energies are in excellent agreement with the experimental torsion barrier for the trans → cis isomerization (11.6 ± 0.2 kcal/mol[2]).

2. Potential Energy Surface and Reaction Coordinate. The intrinsic reaction coordinate for the trans → cis isomerization was evaluated with a 0.01 au step. The reaction coordinate is defined by the minimum energy path that connects the reactants to the products and passes through the transition state. The reaction path is determined by the nonstationary points calculated in both directions from the saddle point. Figure 1 shows the reaction paths calculated at MP2 and B3LYP levels and using the D95V(d,p), 6-31G(d,p), and 6-311G(d,p) basis sets. In this paper, the reaction coordinate, *s*, is expressed in atomic units, as usual. The calculated reaction paths have the shape of an inverted symmetric parabolic-like potential curve with a small curvature.

Variations of the internal coordinates with the reaction coordinate at MP2/6-31G(d,p) level of theory are shown in Figure 2. The results at other levels are quite similar, so they

TABLE 3a: Calculated Energies (hartrees) and Zero-Point Vibrational Energies (kcal/mol) for *cis*-HONO, *trans*-HONO, and the Saddle Point

	energies (hartrees)			zero-point vibrational energies (kcal/mol)		
	cis-HONO	*trans*-HONO	saddle point	*cis*-HONO	*trans*-HONO	saddle point
RHF/D95V(d,p)	−204.695933	−204.694163	−204.676720	14.602	14.488	13.267
MP2/D95V(d,p)	−205.219699	−205.218496	−205.198952	12.744	12.608	11.154
full-MP2/D95V(d,p)	−205.227664	−205.226454	−205.206811	12.764	12.629	11.178
MP2/6-31G(d,p)	−205.177870	−205.176080	−205.156175	12.809	12.679	11.238
B3LYP/D95V(d,p)	−205.750501	−205.749587	−205.728741	12.758	12.762	11.443
B3LYP/6-31G(d,p)	−205.701723	−205.700290	−205.679006	12.821	12.799	11.464
B3LYP/6-311G(d,p)	−205.762150	−205.761768	−205.741044	12.724	12.749	11.416

TABLE 3b: Calculated Thermodynamic Values for the *trans*-HONO → *cis*-HONO Isomerization (298 K)

	ΔH (kcal/mol)	S_{cis} (cal/mol K)	S_{trans} (cal/mol K)	ΔS (cal/mol K)	ΔG (kcal/mol)	E_0 (kcal/mol)	$\Delta S^{\ddagger}$ (cal/mol K)	$\Delta G^{\ddagger}$ (kcal/mol)
RHF/D95V(d,p)	−0.997	58.61	58.75	−0.14	−0.955	9.725	−0.421	9.850
MP2/D95V(d,p)	−0.619	59.13	59.38	−0.25	−0.544	10.810	−0.179	10.863
full-MP2/D95V(d,p)	−0.624	59.11	59.37	−0.26	−0.547	10.875	0.064	10.856
MP2/6-31G(d,p)	−0.993	59.05	59.31	−0.26	−0.916	11.050	0.039	11.038
B3LYP/D95V(d,p)	−0.578	59.10	59.31	−0.21	−0.515	11.762	−0.344	11.865
B3LYP/6-31G(d,p)	−0.877	59.03	59.27	−0.24	−0.806	12.021	−0.110	12.054
B3LYP/6-311G(d,p)	−0.265	59.06	59.30	−0.24	−0.193	11.672	−0.095	11.700

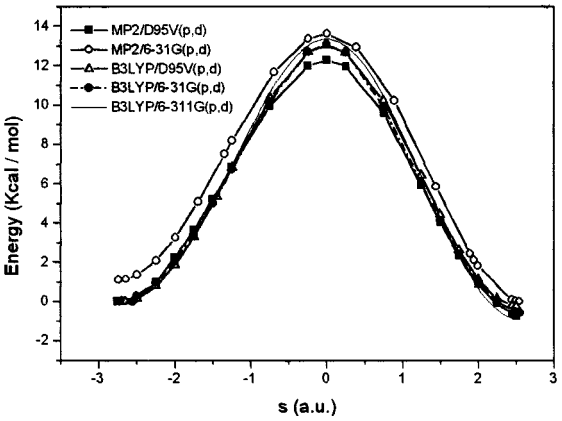

Figure 1. Minimum energy paths calculated for the *trans*-HONO → *cis*-HONO isomerization at MP2 and B3LYP levels with D95V(d,p) and 6-31G(d,p) basis sets.

are not presented. A large variation in the torsion angle is observed as the reaction coordinate is increased. The N−O distance and HNO and ONO angles vary 3% along the reaction path, while the other internal coordinates show even smaller deviations, less than 1%.

The change in vibrational frequencies on the reaction path is shown in Figure 3. Note that the stretching and bending modes are conserved, while the torsion mode is lost in the range of the reaction coordinate, *s*, which varies from −1 to 1 au.

The vibrational frequencies and the geometry variations on the reaction path suggest that the reaction coordinate is mainly the torsion angle and that isomerization occurs by an out-of-plane rotation of the O−H bond. Moreover, the detailed dynamics of the geometric isomerization of nitrous acid (*trans*-HONO → *cis*-HONO) is as follows: initially, the N═O bond distance decreases, the N−O bond distance increases, and the O−H bond rotates, reaching the saddle point, which then relaxes to the product *cis*-HONO by decreasing the N−O bond distance, increasing the N═O bond distance, and completing the 180° rotation.

3. Rate Constants. Assuming that intramolecular vibrational energy transfer in nitrous acid occurs on a time scale fast enough to allow RRKM behavior, we determined the microcanonical rate constants, $k(E,J)$, for the isomerization of *trans*-HONO → *cis*-HONO on the basis of this theory. Since this isomerization is an IV-photoinduced process, knowing the microcanonical rate constants is of great importance. The direct-count Beyer−Swinehart algorithm[30] was used to evaluate the sum and density of states. An upper limit of 40 kcal/mol was used for the evaluation of the microcanonical rate constants. This value was chosen because at higher energies, nitrous acid undergoes dissociation into HO and NO radicals[31]. Figure 4 shows *J*-averaged $k(E,J)$ rate constants determined from the different data obtained from theoretical calculations.

The microcanonical $k(E,J)$ rate constants determined from the MP2/6-31G(d,p) ab initio data show a small dependence with the *J* value.[32] Microcanonical variational $k(E,J)$ rate constants were also evaluated, but no significant variational effect was observed. The variational microcanonical rate constants are about 1% lower, in agreement with previous canonical variational transition-state theory rate constants (CVTST) calculated at the HF level.[33]

The high-pressure unimolecular rate constants,[34] $k(T)$, were evaluated as canonical mean values for *J*-averaged k(E,J) microcanonical rate constants by considering a Boltzmann distribution. In this way, the high-pressure unimolecular rate constants are equivalent to TST rate constants.[26c] The values obtained for $k(T)$ show good agreement with the rate constants computed in our laboratory using CVTST,[33] which suggests that the variational effect is unimportant for this reaction. Over the temperature range from 223 to 323K, the calculated isomerization rate constants fit the Arrhenius form $A \exp(-E_a/RT)$, where *A* is the pre-exponential factor and E_a is the activation energy. The Arrhenius forms presented in Table 4 are in good agreement with the previously estimated[13] Arrhenius form, $1.33 \times 10^{13} \exp(-10.9/RT)$, obtained from parametrized values of molecular properties and barrier height. Similar values for the activation energy were obtained from the different levels of theory employed. The activation energies and critical energies are nearly the same, since the thermal correction (RT) is around 0.5 kcal/mol.

The critical energies obtained at MP2/D95V(d,p) and full-MP2/D95V(d,p) levels differ by about 0.06 kcal/mol, which could suggest that the frozen core approach is adequate for the quantum mechanical description of this reaction. The rate constants calculated from the MP2 data are almost twice those calculated from the full-MP2 data. The latter are similar to those

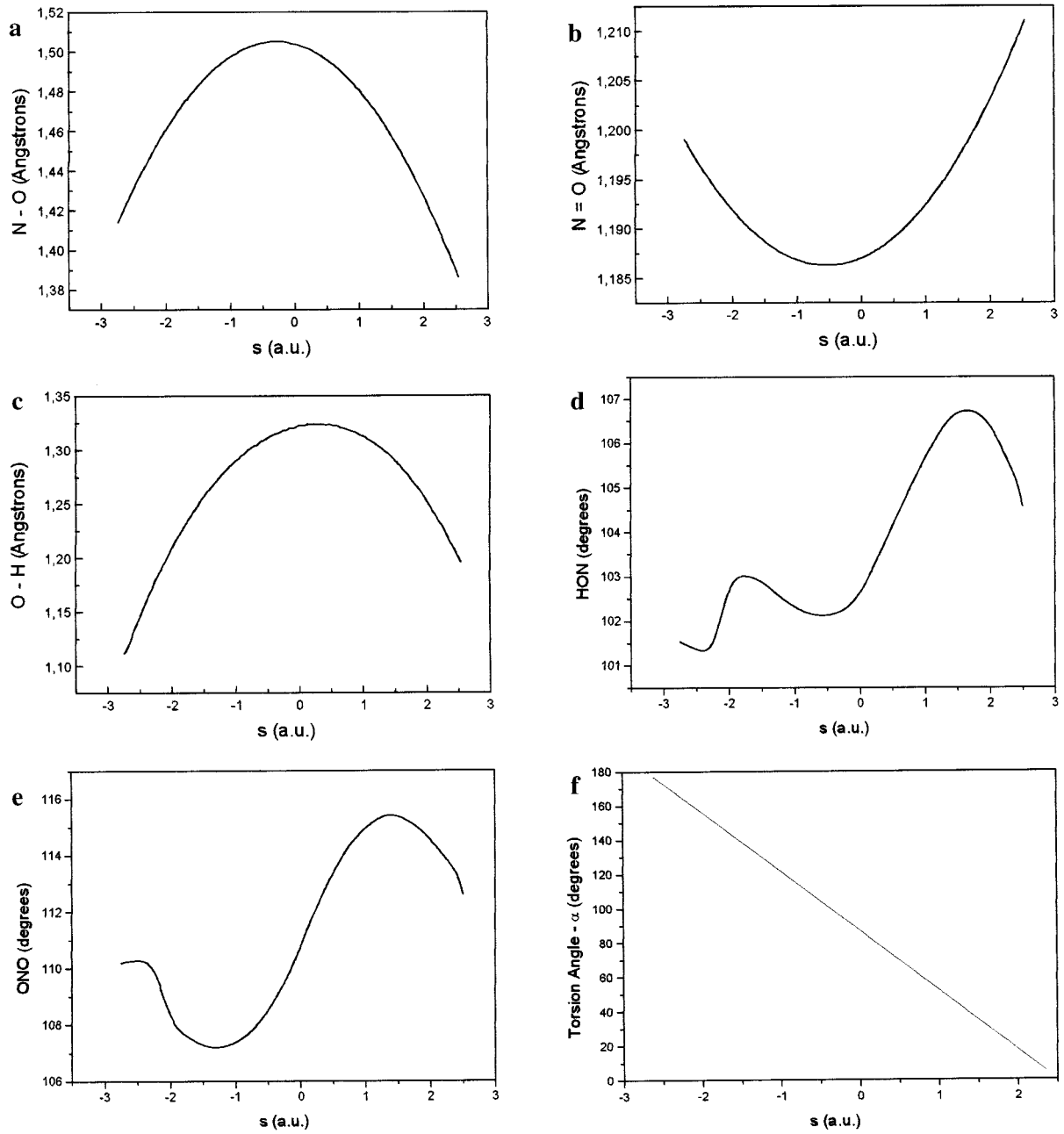

Figure 2. (a) N−O bond distance variation as a function of the reaction coordinate *s* (au), calculated at MP2/6-31G(d,p) level. (b) N═O bond distance variation as a function of the reaction coordinate *s* (au), calculated at MP2/6-31G(d,p) level. (c) O−H bond distance variation as a function of the reaction coordinate *s* (au), calculated at MP2/6-31G(d,p) level. (d) HON angle variation as a function of the reaction coordinate *s* (au), calculated at MP2/6-31G(d,p) level. (e) ONO angle variation as a function of the reaction coordinate *s* (au), calculated at MP2/6-31G(d,p) level. (f) Torsion angle variation as a function of the reaction coordinate *s* (au), calculated at MP2/6-31G(d,p) level.

obtained when the basis set D95V(d,p) was changed to 6-31G-(d,p) at the MP2 level. Similar behavior is observed when the basis sets are changed in the B3LYP calculations: the rate constants determined from the B3LYP/D95V(d,p) data are about twice as large as those obtained from the B3LYP/6-31G(d,p) data, which are three times smaller than the rate constants determined from B3LYP/6-311G(d,p) data. Thus, the choice of basis set affects the final rate constants. Finally, by comparing the values of the rate constants generated from the MP2 and B3LYP calculations for the same basis set, we see that the B3LYP values are approximately 10% smaller. The difference found in rate constants determined from different sets of ab initio data is acceptable if common experimental errors for thermal reactions are considered, since an error of 1 kcal/mol in the barrier height leads to a 5-fold error in the rate constant.

Tunneling corrections were estimated using semiclassical Wigner correction

$$\kappa^{W}(T) = 1 + \frac{1}{24}\left|\frac{\hbar\nu}{K_B T}\right|^2$$

where κ^{W} is the transmission coefficient, ν is the imaginary frequency, and K_B is the Boltzmann constant. The tunneling-corrected rate constant, $k^{W}(T)$, is then obtained by multiplying $k(T)$ with κ^{W}. Wigner transmission coefficients lie in the range from 1.009 to 1.011, showing that tunnel effect increases the rate of this reaction by a factor of 1%.

Conclusions

This paper uses the direct dynamics method to study the nitrous acid cis−trans isomerization. With this methodology,

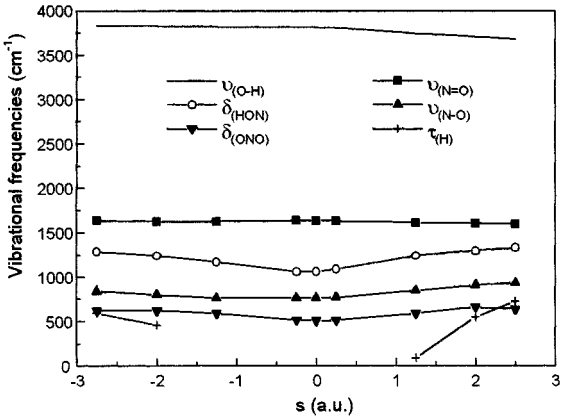

Figure 3. Vibrational frequency variation as a function of the reaction coordinate *s* (au), calculated at MP2/6-31G(d,p) level.

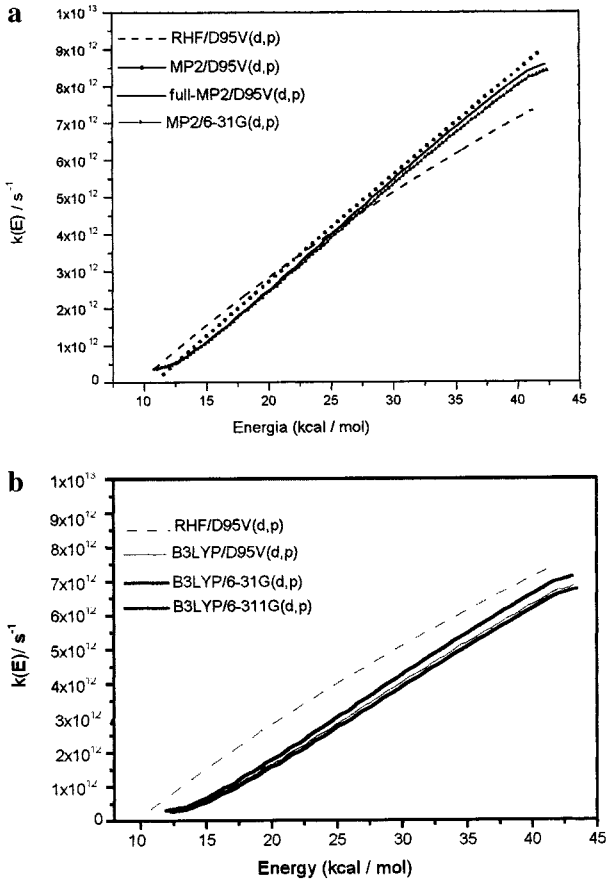

Figure 4. (a and b) Microcanonical RRKM rate constant, $k(E)$ (s^{-1}), as a function of internal energy (kcal/mol).

we obtained a microscopic description of the reaction dynamics and determined the rate constants. To the best of our knowledge, these calculations seem to be the first complete quantitative determination of RRKM and TST rate constants for this system to date.

Comparable results are obtained for electronic structure and energy differences using both the MP2 and DFT levels of theory, suggesting that the DFT level may be used for larger systems, or at least for this kind of reaction, with a considerable reduction of computational effort.

Small variational effects are observed for both the microcanonical RRKM and CVTST rate constants. The tunneling effect was also evaluated and was proved to be unimportant for this reaction.

TABLE 4: Arrhenius Parameters for *trans*-HONO → *cis*-HONO[a]

	$k(T) = A \exp(-E_a/RT)$	
level of theory	A	E_a
RHF/D95V(d,p)	1.49×10^{13}	10.50
MP2/D95V(d,p)	1.69×10^{13}	11.37
full-MP2/D95V(d,p)	1.70×10^{13}	11.66
MP2/6-31G(d,p)	1.58×10^{13}	11.62
B3LYP/D95V(d,p)	1.52×10^{13}	12.49
B3LYP/6-31G(d,p)	1.54×10^{13}	12.78
B3LYP/6-311G(d,p)	1.56×10^{13}	12.21

[a] Preexponential factor A in s^{-1} and activation energy (E_a) in kcal/mol.

Supporting Information Available: Table 5S lists the values of $k(E,J)$ computed for *trans*-HONO → *cis*-HONO from 12 to 40 kcal/mol and with J quantum numbers from 0 to 20 using MP2/6-31G(d,p) ab initio input data. Inclusion of the rotational quantum number J causes the rate constants to decrease less than 5% for $J < 5$, but this effect is increased at low energies and high values of J. Rate constants decrease more than 20% for energies lower than 15 kcal/mol and $J > 10$. Table 6S shows a list of unimolecular high-pressure rate constants calculated from 273 to 373 K using different ab initio input data.

Acknowledgment. The authors thank Dr. Maria Cristina Rodrigues da Silva for her contribution and helpful discussions, Professor W. L. Hase for providing a computational code for the evaluation of variational microcanonical rate constants, and Professor D. Truhlar, for providing the POLYRATE program. The authors also thank CNPq and CAPES for partial financial support.

References and Notes

(1) Cox, A. P.; Brittain, A. H.; Finnigan, D. J. *Trans. Faraday Soc.* **1971**, *67*, 2179.
(2) Mcgraw, G. E.; Bernitt, D. L.; Hisatsune, I. C. *J. Chem. Phys.* **1966**, *45*, 1392.
(3) Hall, R. T.; Pimentel, G. C. *J. Chem. Phys.* **1963**, *38*, 1889.
(4) McDonald, P. A.; Shirk, J. S. *J. Chem. Phys.* **1982**, *77*, 2355.
(5) Cárdenas-Jirón, G. I.; Cárdenas-Lailhacar, C.; Toro-Labbé, A. *J. Mol. Struct.* (*THEOCHEM*) **1990**, *210*, 279.
(6) Cárdenas-Jirón, G. I.; Lahsen, J.; Toro-Labbé, A. *J. Phys. Chem.* **1995**, *99*, 5325.
(7) Cárdenas-Jirón, G. I.; Toro-Labbé, A. *J. Phys. Chem.* **1995**, *99*, 12730.
(8) Lee, T.; Rendel, A. P. *J. Chem. Phys.* **1991**, *94*, 6229.
(9) Radom, L.; Hehre, W. J.; Pople, J. A. *J. Am. Chem Soc.* **1971**, *93*, 289.
(10) Darsey, J. A.; Thompson, D. L. *J. Phys. Chem.* **1987**, *91*, 3168.
(11) Skaarup, S.; Boggs, J. E. *J. Mol. Struct.* **1976**, *30*, 389.
(12) Turner, A. G. *J. Phys. Chem.* **1985**, *89*, 4480.
(13) Benioff, P.; Das, G.; Wahl, A. C. *J. Chem. Phys.* **1976**, *64*, 710.
(14) Turner, A. G. *J. Phys. Chem.* **1985**, *89*, 4480.
(15) Coffin, J. M.; Pulay, P. *J. Phys. Chem.* **1991**, *95*, 118.
(16) Cárdenas-Jirón, G. I.; Toro-Labbé, A. *An. Quim.* **1992**, *88*, 43.
(17) Hisatsune, I. C. *J. Phys. Chem.* **1968**, *72*, 269.
(18) Truhlar, D. G.; Isaacson, A. D.; Garret, B. C. *Generalized Transition State Theory* in *The Theory of Chemical Reaction Dynamics*; CRC Press: Boca Raton, FL, 1995; Vol. 4, pp 65−137.
(19) Kato, S.; Kato, H.; Fukui, K. *J. Phys. Chem.* **1977**, *99*, 684.
(20) Møller, C. and Plesset, M. S. *Phys. Rev.* **1934**, *46*, 618.
(21) Hohenberg, P. and Kohn, W. *Phys. Rev.* **1964**, *136*, B864.
(22) Becke, A. D. *J. Chem. Phys.* **1993**, *98*, 5648.
(23) Dunning, T. H., Jr.; Hay, P. J. In Modern Theoretical Chemistry; Schaefer, H. F., III, Ed.; Plenum: New York, 1976; pp 1−28.
(24) Ditchfield, R.; Hehre, W. J.; Pople, J. A. *J. Chem. Phys.* **1971**, *54*, 724.
(25) McLean, A. D.; Chandler, G. S. *J. Chem. Phys.* **1980**, *72*, 5639.
(26) (a) Forst, W. *Theory of Unimolecular Reactions*; Academic Press: New York, 1973. (b) Robinson, P. J.; Holbrook, K. H. *Unimolecular*

Reactions. Wiley-Interscience: New York, 1972. (c) Steinfeld, J. I.; Francisco, J. S.; Hase, W. L. *Chemical Kinetics and Dynamics*, 2nd ed.; Prentice Hall: New York, 1998. (d) Gilbert, R. G.; Smith, S. C. *Theory of Unimolecular and Recombination Reactions*; Blackwell Scientific Publications: Cambridge, MA, 1990.

(27) Schlegel, H. B. Geometry Optimization on Potential Energy Surfaces. In *Modern Electronic Structure Theory*; World Scientific Publishing: New York, 1994; Vol. 2.

(28) Frisch, M. J.; Trucks, G. W.; Schlegel, H. B.; Gill, P. M. W.; Johnson, B. G.; Robb, M. A.; Cheeseman, J. R.; Keith, T. A.; Peterson, G. A.; Montgomery, J. A.; Ragavachari, K.; Al-Laham, M. A.; Zakrewski, V. G.; Ortiz, J. V.; Foresman, J. B.; Cioslowski, J.; Stefanov, B. B.; Nanayakkara, A.; Challacombe, M.; Peng, C.; Ayala, P. Y.; Chen, W.; Wong, M. W.; Andres, J. L.; Replogle, E. S.; Gomperts, R.; Martin, R. L.; Fox, D. J.; Binkley, J. S.; Defrees, D. J.; Baker, J.; Stewart, J. P.; Head-Gordoon, M.; Gonzales, C.; Pople, J. A. *GAUSSIAN 94*, Revision E.2; Gaussian, Inc.: Pittsburgh, PA, 1995.

(29) Deeley, C. M.; Mills, I. M. *Mol. Phys.* **1985**, *54*, 23.

(30) Beyer, T.; Swinehart, D. F. *Comm. Assoc. Comput. Machines* **1973**, *16*, 379.

(31) Baulch, D. L.; Cox, R. A.; Crutzen, P. J.; Hampson, R. F., Jr.; Kerr, J. A.; Troe, J.; Watson, R. T. *J. Phys. Chem. Ref. Data* **1982**, *11*, 327.

(32) Microcanonical rate constants, $k(E,J)$, are available as Supporting Information in Table 5S.

(33) Bauerfeldt, G. F. M. Sc. Thesis, Universidade Federal do Rio de Janeiro, Rio de Janeiro, Brazil, 1999.

(34) High-pressure unimolecular rate constants, $k(T)$, are are available as Supporting Information in Table 6S.